



1 **Dry and warm conditions in Australia exacerbated by aerosol reduction in China**

2

3

4

5

6 Jiyuan Gao<sup>1</sup>, Yang Yang<sup>1\*</sup>, Hailong Wang<sup>2</sup>, Pinya Wang<sup>1</sup>, Hong Liao<sup>1</sup>

7

8

9

10

11

12

13

14 <sup>1</sup>Joint International Research Laboratory of Climate and Environment Change (ILCEC), Jiangsu

15 Key Laboratory of Atmospheric Environment Monitoring and Pollution Control, Jiangsu

16 Collaborative Innovation Center of Atmospheric Environment and Equipment Technology,

17 School of Environmental Science and Engineering, Nanjing University of Information Science

18 and Technology, Nanjing, Jiangsu, China

19 <sup>2</sup>Atmospheric, Climate, and Earth Sciences Division, Pacific Northwest National Laboratory,

20 Richland, Washington, USA

21

22

23

24

25

26 \*Correspondence to [yang.yang@nuist.edu.cn](mailto:yang.yang@nuist.edu.cn)

27



28 **Abstract**

29 A substantial decline in anthropogenic aerosols in China has been observed since the initiation of  
30 clean air actions in 2013. Concurrently, Australia experienced anomalously dry and warm  
31 conditions in 2010s. This study reveals a linkage between aerosol reductions in China and the  
32 drying and warming trends in Australia during 2013–2019 based on aerosol-climate model  
33 simulations and multi-source observations. Aerosol decline in China triggered alterations in  
34 temperature and pressure gradients between the two hemispheres, leading to intensified outflow  
35 from Asia towards the South Indian Ocean, strengthening the Southern Indian Subtropical High  
36 and its related Southern Trade Winds. Consequently, this atmospheric pattern resulted in a  
37 moisture divergence over Australia. The reduction in surface moisture further resulted in more  
38 surface energy being converted into sensible heat instead of evaporating as latent heat, warming  
39 the near-surface air. Aerosol reductions in China are found to contribute to 19% of the observed  
40 decreases in precipitation and relative humidity and 8% of the increase in surface air temperature  
41 in Australia during 2013–2019. The intensified dry and warm climate conditions during 2013–  
42 2019 further explain 12%–19% of the increase in wildfire risks during fire seasons in Australia.  
43 Our study illuminates the impact of distant aerosols on precipitation and temperature variations in  
44 Australia, offering valuable insights for drought and wildfire risk mitigation in Australia.

45



## 46 **1 Introduction**

47 Australia encompasses various climate zones, ranging from the tropical climate in the north  
48 to arid conditions in the interior and temperate climates in the south (Head et al., 2014). The  
49 continent is predominantly dry, receiving an average annual rainfall of less than 600 mm and less  
50 than 300 mm over half of the land. Evident long-term trends can be observed in Australia's  
51 historical rainfall records. These trends reveal a notable shift towards drier conditions across  
52 southern Australia (Dey et al., 2019a; Nicholls, 2006; Rauniyar and Power, 2020; Wasko et al.,  
53 2021), and an increase in rainfall before 2010 (Dey et al., 2019a, b; Evans et al., 2014; Nicholls,  
54 2006; Rotstayn et al., 2007; Wasko et al., 2021) followed by a slight decreasing trend of rainfall  
55 after 2010 (CSIRO and BOM, 2022) in the northern Australia.

56 Precipitation in Australia is influenced by a variety of atmospheric circulation systems,  
57 including East Coast Lows (ECLs), the Australian-Indonesian Monsoon, tropical cyclones (TCs),  
58 fronts, and different modes of large-scale climate variabilities, such as the El Niño-Southern  
59 Oscillation (ENSO), Indian Ocean Dipole (IOD), Interdecadal Pacific Oscillation (IPO),  
60 Subtropical ridge (STR), Southern Annular Mode (SAM), and Madden Julian Oscillation (MJO)  
61 (Dey et al., 2019a; Risbey et al., 2009). The linkages between Australia's rainfall characteristics  
62 and these drivers could change in response to the internal natural variabilities and external  
63 anthropogenic forcings. Rauniyar and Power (2020) reported that the drier conditions across the  
64 southern Australia could be attributed to a combination of both decadal-scale natural variability  
65 and changes in large-scale atmospheric circulation patterns, which was linked to the escalating  
66 emissions of greenhouse gases (GHGs), while Rotstayn et al. (2007) found that the increased levels  
67 of rainfall in northern Australia before 2010 was linked to the increases in aerosols in Asia.

68 Human activities have led to a rise of global surface air temperature by approximately 1.29 °C  
69 (0.99 to 1.65 °C) from 1750 to 2019, mainly due to an enhanced greenhouse effect from increasing  
70 GHGs (IPCC, 2021). In addition to GHGs, human activities also emit a variety of aerosols and  
71 their gaseous precursors into the atmosphere. Since industrialization, there has been a significant  
72 rise in the levels of aerosols and precursors (Hoesly et al., 2018). These atmospheric aerosols play  
73 a crucial role in changing the earth's radiation balance, both directly and indirectly, and are  
74 considered as the second-largest anthropogenic climate forcer following GHGs, exerting an overall



75 cooling effect that masks the warming induced by GHGs (IPCC, 2013, 2021). However, as  
76 anthropogenic aerosols declined during the past decades in many countries of the world related to  
77 the clean air actions, the associated “unmask” effect is likely to exacerbate GHG-induced warming  
78 (Kloster et al., 2010). For example, in the 1980s, clean air actions were implemented in North  
79 America and Europe, leading to a decrease in the emissions of aerosols and their precursors  
80 (Hoesly et al., 2018). Reductions in aerosol emissions in the U.S. have led to changes in aerosol  
81 direct radiative forcing (DRF) by  $0.8 \text{ W m}^{-2}$  and indirect radiative forcing (IRF) by  $1.0 \text{ W m}^{-2}$  over  
82 the eastern U.S. during 1980–2010 (Leibensperger et al., 2012). Similarly, aerosol decreases over  
83 Europe between the 1980s and 1990s have caused a change in regional DRF by  $1.26 \text{ W m}^{-2}$   
84 (Pozzoli et al., 2011). In China, the emissions of aerosols and their precursors have been reduced  
85 since 2013 due to the implementation of Air Pollution Prevention and Control Action Plan. Dang  
86 and Liao (2019) reported a  $1.18 \text{ W m}^{-2}$  change in DRF between 2012 and 2017 due to decreased  
87 aerosol levels over eastern China. Gao et al. (2022) estimated a warming of  $0.20 \text{ }^\circ\text{C}$  in China,  
88  $0.15 \text{ }^\circ\text{C}$  in North America, and  $0.14 \text{ }^\circ\text{C}$  in Europe, attributed to the decreases in aerosols during  
89 2013–2019.

90 Monsoonal rainfall serves as a vital resource for agriculture, industry, and ecosystems across  
91 the monsoon-affected regions, affecting approximately two-thirds of the world’s population (B.  
92 Wang et al., 2021). Apart from GHGs-induced warming (Cook and Seager, 2013) and nature  
93 variabilities (e.g., ENSO) (Oh and Ha, 2015), aerosol also modulates monsoon system mainly  
94 through changing land-sea temperature and pressure gradient. The impact of aerosols on Asian  
95 monsoon has been widely investigated. Based on climate model simulations, Liu et al. (2023)  
96 found that aerosol reductions in East Asia during 2013–2017 resulted in an approximately 5%  
97 increase in the strength of the East Asian summer monsoon (EASM). The EASM is also reported  
98 to enhance due to future aerosol reductions from 2000 to 2100 (Wang et al., 2016). Dong et al.  
99 (2019) explored the effects of increased aerosol in Asia from 1970s to 2000s on atmospheric  
100 circulation and rainfall patterns and found anomalous moisture convergence and increased  
101 precipitation over the Maritime continent. Non-Asian aerosols also have an effect on South Asian  
102 monsoon rainfall through changes in the interhemispheric temperature gradient and meridional  
103 shifts of the Intertropical Convergence Zone (Bollasina et al., 2011, 2014; Cowan and Cai, 2011;  
104 Undorf et al., 2018). Australia, especially the northern Australia, is largely affected by Australian  
105 monsoon, which is characterized by winds that blow from the southeast during cold season and



106 from the northwest during the warm season (Gallego et al., 2017; Heidemann et al., 2023).  
107 Australia has a relatively low level of anthropogenic aerosols, which suggests that the impact of  
108 domestic anthropogenic aerosols on Australian monsoon should not be significant. However, the  
109 impact of remote aerosols on Australian monsoon have been investigated in previous studies, and  
110 they reported that the increases in Asian aerosols could enhance rainfall in Australia through  
111 increasing monsoonal winds towards Australia (Rotstayn et al., 2007; Fahrenbach et al., 2023).

112 Wildfires, which are uncontrolled fires spreading rapidly across natural landscapes, are  
113 significantly influenced by meteorological conditions (He et al., 2019; Jones et al., 2022). In  
114 Australia, these fires, also known as bushfires, present a major environmental and social threat  
115 (Johnston et al., 2021; Ward et al., 2020). According to Dowdy (2020), the most favorable seasons  
116 for wildfires in most regions of Australia are austral spring and summer. Key meteorological  
117 factors such as extended periods of drought, elevated temperatures, low humidity, and strong winds  
118 are crucial in determining the occurrence and intensity of wildfires (Zacharakis and Tsihrintzis,  
119 2023). Under the recent historical climate change, Australia has witnessed a rise in extreme fire  
120 weather conditions and an extended fire season (CSIRO and BOM, 2022).

121 Since the implementation of clean air policies in 2013, there has been a noticeable decrease  
122 in aerosol levels in China (Zhang et al., 2019; Zheng et al., 2018). Numerous studies have shown  
123 the local and global climate effects of the aerosol reductions in China (Dang and Liao, 2019; Gao  
124 et al., 2022, 2023; Liu et al., 2023; Zheng et al., 2020). The Australian monsoonal wind patterns,  
125 reported to be influenced by Asian aerosol emissions in the past decades (Rotstayn et al., 2007;  
126 Fahrenbach et al., 2023), may have also influenced by the radiative effects due to the aerosol  
127 decline in China. The objective of this study is to assess the worsened dry and warm conditions  
128 and associated wildfire risk in Australia during 2013–2019 and investigate the possible linkage  
129 between the changes in climate conditions in Australia and anthropogenic aerosols.

## 130 **2 Methods**

### 131 **2.1 Observational and Reanalysis Data**

132 Ground-based observational data of near-surface  $PM_{2.5}$  concentrations in China 2013–2019  
133 are acquired from the China National Environmental Monitoring Centre (CNEMC), which offers



134 daily records of near-surface air pollutant concentrations for nearly 1800 sites. Aerosol Optical  
135 Depth (AOD) data are obtained from the Moderate Resolution Imaging Spectroradiometer  
136 (MODIS) Deep Blue retrieval (Hsu et al., 2013). These observational data are used for evaluating  
137 the performance of model simulated aerosols.

138 ERA5, the fifth generation of the European Centre for Medium-range Weather Forecasts  
139 (ECMWF) atmospheric reanalysis, is a comprehensive dataset that provides a detailed and globally  
140 consistent view of the earth's atmospheric conditions over the past several decades (Hersbach et  
141 al., 2020). In this study, ERA5 data are employed to evaluate the climate condition in Australia  
142 and analyze its linkage with aerosol reductions in China during the 2013–2019 by using the 2-  
143 meter temperature, total precipitation, relative humidity, cloud cover, wind fields, vertical velocity,  
144 surface latent and sensible heat flux, and surface and top of the atmosphere (TOA) solar and  
145 longwave radiative flux under both clear and all sky conditions.

146 Clouds and the Earth's Radiant Energy System-Energy Balanced and Filled (CERES-EBAF)  
147 is a dataset that provides information on the earth's radiation budget, including surface and TOA  
148 energy fluxes (Loeb et al., 2018). It combines data from satellite instruments to estimate how much  
149 energy the earth receives from the sun and how much is reflected back to space, helping to  
150 understand climate change and energy balance processes. The variables used in the study include  
151 cloud cover and surface and TOA solar and longwave radiative fluxes under both clear and all sky  
152 conditions.

153 The Global Precipitation Measurement (GPM) mission is a joint initiative by National  
154 Aeronautics and Space Administration (NASA) and the Japan Aerospace Exploration Agency  
155 (JAXA) aimed at providing accurate and frequent measurements of global precipitation  
156 (Skofronick-Jackson et al., 2017). GPM includes a core satellite equipped with advanced radar and  
157 microwave sensors, enabling the observation of rain and snowfall in real-time. The data are crucial  
158 for understanding weather patterns, climate dynamics, and hydrological processes. Precipitation  
159 rate data from GPM are also used in the study.



## 160 **2.2 Model Description and Experimental Design**

161 In this research, we conduct simulations to explore the impact of aerosols on climate using  
162 the Community Earth System Model version 1 (CESM1). CESM1 simulates the major aerosols  
163 including sulfate, black carbon (BC), primary organic matter (POM), secondary organic aerosol  
164 (SOA), dust and sea salt in a four-mode Modal Aerosol Module (MAM4), as described in Liu et  
165 al. (2016). CESM1 simulations are carried out with 30 vertical layers and a horizontal resolution  
166 of 2.5° longitude by 1.9° latitude. In addition to the default model physics, several supplementary  
167 features are incorporated into the model in this study to improve the model's performance in  
168 simulating aerosol wet scavenging and convective transport (Wang et al., 2013).

169 The global anthropogenic emissions of aerosols and their precursors are obtained from the  
170 Community Emissions Data System (CEDS) v\_2021\_04\_21. In contrast to the prior CEDS  
171 v\_2016\_07\_26, which exhibits significant regional emission biases (Z. Wang et al., 2021), the  
172 newer CEDS version of anthropogenic emissions of aerosols and precursors considers the  
173 substantial reductions in emissions in China, related to the recent clean air actions since 2013 (Fig.  
174 S1). Specifically, anthropogenic sulfur dioxide (SO<sub>2</sub>), BC, and organic carbon (OC) emissions  
175 decreased by -12.48, -0.30, and -0.21 Tg yr<sup>-1</sup>, respectively, over China between 2013 and 2019.  
176 Biogenic emissions are from the Model of Emissions of Gases and Aerosols from Nature version  
177 2.1 (MEGAN v2.1) (Guenther et al., 2012), while the emissions from open biomass burning are  
178 derived from the CMIP6 (Coupled Model Intercomparison Project Phase 6) (Van Marle et al.,  
179 2017).

180 A series of model experiments are conducted using CESM1 with a fully-coupled model  
181 configuration, as detailed in Table S1. In the baseline scenario (referred to as BASE),  
182 anthropogenic emissions of aerosols and precursors are fixed at year 2013 worldwide. In CHN,  
183 anthropogenic emissions of aerosols and precursors over China are fixed at year 2019, while  
184 emissions in all other regions are remained at year 2013. In NAEU, the simulation is performed  
185 with anthropogenic emissions of aerosols and precursors over North America and Europe set at  
186 year 2019, while emissions in other regions remained at year 2013. In OTH, anthropogenic  
187 emissions of aerosols and precursors in other regions except for China are set at year 2019, while  
188 emissions in China are kept at year 2013. Biogenic and biomass burning emissions worldwide in



189 all experiments are fixed at year 2013. To reduce model biases related to internal variability, three  
190 ensemble members are conducted by perturbing the initial atmospheric temperature conditions.  
191 All simulations are run for 150 years, with the last 100 years for detailed analysis.

### 192 **2.3 Model Evaluation**

193 To validate whether CESM1 can reproduce the aerosol reductions in China during the 2010s,  
194 changes in simulated near-surface  $PM_{2.5}$  concentrations (sum of sulfate, BC, POM, SOA, dust $\times$ 0.1,  
195 and sea-salt $\times$ 0.25 following Turnock et al. (2020)) in China during 2013–2019 are compared with  
196 the observations. Figure S2 shows spatial distributions of observed and modeled annual mean near-  
197 surface  $PM_{2.5}$  concentration changes over China (2017–2019 minus 2013–2015), which exhibited  
198 a statistically significant correlation coefficient of 0.52 between simulations and observations.  
199 However, the model underestimates the  $PM_{2.5}$  concentration changes by 76% in China. The  
200 considerable underestimation has been reported in many previous studies, resulting from coarse  
201 model resolution, uncertainties in emissions of aerosols and precursor gases, strong aerosol wet  
202 removal, and the model’s deficiency in simulating nitrate and ammonium aerosols (Fan et al., 2018,  
203 2022; Gao et al., 2022, 2023; Zeng et al., 2021). The model has a good capability in replicating  
204 the spatial distribution of AOD changes in China during 2013–2019 (Fig. S3), as evidenced by a  
205 high correlation coefficient of 0.83, but the model also exhibits an underestimation in the AOD  
206 reductions by 69%.

207 Climate variables, including precipitation rate, surface air temperature, relative humidity,  
208 total cloud cover, surface solar radiation, 10m wind speed, and surface and TOA net total radiative  
209 fluxes under both clear and all sky conditions over Australia simulated by CESM1 model are also  
210 compared with those from ERA5 reanalysis (Fig. S4–S6). The model demonstrates a good  
211 performance in simulating Australian climate, with normalized mean bias (NMB) values  
212 consistently below or near 40% for surface air temperature, relative humidity, total cloud cover,  
213 surface downward solar radiation, and 10m wind speed, and surface and TOA net total radiative  
214 fluxes, but it tends to overestimate annual precipitation by about 90%, especially over coastal  
215 regions likely related to the coarse model resolution. The model accurately reproduces spatial  
216 patterns of all climate variables, closely aligning with observations, as indicated by correlation  
217 coefficients ranging from 0.7 to 1.0.





## 218 **2.4 Wildfire Risk Indices**

219 In this study, several climatological indices are used to indicate wildfire risk during fire  
220 seasons (austral spring and summer, from September to February of the next year) in Australia  
221 (Ren et al., 2022; Irmak et al., 2003; Seager et al., 2015; Sharples et al., 2009).

222 (i) Reference Potential Evapotranspiration ( $ET_0$ ):

223  $ET_0$  is a climatological index used to estimate the amount of water that could potentially  
224 evaporate and be transpired from the earth's surface under specific meteorological conditions. The  
225 calculation of  $ET_0$  takes into account factors such as temperature ( $T$ , unit: °C), and surface  
226 downward solar radiation ( $R_s$ , unit:  $W m^{-2}$ ) to estimate the maximum amount of water loss due to  
227 evaporation and transpiration.  $ET_0$  is important in wildfire studies because it helps to gauge the  
228 environmental moisture conditions and the potential for drought, which can be a significant factor  
229 in wildfire risks assessment.  $ET_0$  is given by the following expression (Irmak et al., 2003):

$$230 \quad ET_0 = -0.611 + 0.149R_s + 0.079T$$

231 (ii) Vapor Pressure Deficit (VPD):

232 Vapor Pressure Deficit (VPD) is a meteorological parameter that measures the difference  
233 between the amount of moisture in the air and the maximum amount of moisture the air can hold  
234 at a given temperature ( $T$ , unit: °C) and moisture (relative humidity,  $RH$ , unit: %). High VPD  
235 values indicate that the air is dry. VPD is important in the context of wildfires because it reflects  
236 the drying potential of the atmosphere. When VPD is high, it can lead to rapid moisture loss from  
237 vegetation, making it more susceptible to ignition and increasing the risk of wildfires. VPD is  
238 given by (Seager et al., 2015):

$$239 \quad VPD = \frac{100 - RH}{100} \times 610.7 \times 10^{\frac{7.5T}{237.3+T}}$$

240 (iii) McArthur Forest Fire Danger Index (FFDI):

241 The McArthur Forest Fire Danger Index (FFDI) is a widely used index in Australia to assess  
242 the potential for bushfires and forest fires. It takes into account various meteorological factors,



243 including T (unit: °C), RH (unit: %), wind speed (U, unit: m s<sup>-1</sup>), and drought factor (DF, unitless).  
244 We set DF as 10 here following Sharples et al. (2009). The FFDI provides a numerical rating that  
245 indicates the level of fire danger, with higher values corresponding to greater fire risks. This index  
246 is particularly valuable for assessing the immediate risk of wildfires and is commonly used in fire  
247 management and prediction. FFDI is defined as (Sharples et al., 2009):

$$248 \quad FFDI = 2e^{-0.45+0.987\ln DF+0.0338T-0.0345RH+0.0234U}$$

### 249 **3 Results**

#### 250 **3.1 Intensified Dry and Warm Conditions in Australia by aerosol changes**

251 Figure 1 shows simulated responses in annual and seasonal precipitation rate, surface air  
252 temperature and relative humidity in Australia to changes in anthropogenic emissions of aerosols  
253 and precursors in China. In response to aerosol reductions in China, Australia experiences  
254 significant decreases in precipitation and relative humidity, while the temperature has an increase  
255 from 2013 to 2019. On regional average, annual precipitation, surface air temperature and relative  
256 humidity change by  $-0.10 \text{ mm day}^{-1}$ ,  $0.08 \text{ °C}$ , and  $-1.19\%$ , respectively, in Australia caused by  
257 the aerosol reduction in China during this time period, contributing to the dry and warm climate in  
258 Australia. Notably, Northern Australia experiences the most significant reduction in convective  
259 precipitation, whereas Southern Australia has the greatest decline in large-scale precipitation  
260 related to the aerosol reduction in China, as simulated by the CESM1 model (Fig. S7). The  
261 direction of seasonal responses in precipitation rate, surface air temperature and relative humidity  
262 are the same as the annual averages, with the largest changes occurring in austral spring (Fig. 1).

263 The intensified dry and warm conditions in Australia can also be seen in the observations,  
264 as indicated by ERA5 reanalysis data (Fig. 2). Since 2010, precipitation and relative humidity have  
265 significantly decreased in Australia, especially in Northern and Eastern Australia, at a rate of  $0.086$   
266  $\text{mm day}^{-1} \text{ yr}^{-1}$  and  $1.07\% \text{ yr}^{-1}$ , respectively, while surface air temperature has increased at a rate  
267 of  $0.17 \text{ °C yr}^{-1}$ . The decrease in precipitation in Australia is also reflected in the GPM data (Fig.  
268 S8). It translates into the changes in precipitation, temperature and relative humidity by  $0.52 \text{ mm}$   
269  $\text{day}^{-1}$ ,  $1.0 \text{ °C}$  and  $6.4\%$  in Australia during 2013–2019 in observations if the trends are assumed to  
270 be linear. This suggests that aerosol reductions in China can explain 19% of the decreases in



271 precipitation and relative humidity and 8% of the increase in surface air temperature in Australia  
272 during 2013–2019, worsening the dry and warm climate conditions in Australia (Fig. S9). The  
273 reduction in anthropogenic SO<sub>2</sub> emissions in China shows strong correlations with the decrease in  
274 precipitation and the increase in temperature in Australia during 2010–2019 (Fig. S10). However,  
275 when extending the time frame to the period before emissions reductions in China (1940–2019),  
276 the increase in temperature becomes less pronounced, with a slight rise in precipitation and relative  
277 humidity, likely attributed to greenhouse gas warming, which can serve as evidence that the  
278 decrease in precipitation and increase in temperature in Australia from 2010 to 2019 are not  
279 primarily caused by GHGs (Figure S11). The rainfall decrease is consistent with changes in clouds.  
280 Spatial distributions of simulated changes in vertically-integrated cloud cover and the linear trends  
281 in observations are shown in Fig. S12–S14. In both observation and model simulation, the results  
282 consistently indicate a reduction in clouds of all levels, including high, mid-level, and low clouds.  
283 In addition, the spatial distributions of these changes closely resemble the patterns of responses in  
284 precipitation and relative humidity.

285 Aerosol emissions have changed across the world rather than in China alone during 2013–  
286 2019, such as those in Australia, North America and Europe, which affect climate in both local  
287 and remote regions. Figures S15a and S15b shows changes in precipitation and surface  
288 temperature in Australia due to changes in other regions except China. The aerosol changes in  
289 other regions except China yield a decrease in precipitation by 0.05 mm day<sup>-1</sup> and an increase in  
290 temperature by 0.08 °C, which are similar to those caused by the aerosol changes in China (Fig.  
291 1). In particular, North America and Europe emission changes largely contribute to the responses  
292 in precipitation (–0.04 mm day<sup>-1</sup>) and temperature (0.08 °C) attributed to other regions (except  
293 China), although the responses are mostly insignificant (Figs. 15c and 15d).

### 294 **3.2 Mechanisms of Dry and Warm conditions in Australia Amplified by Aerosol Reductions** 295 **in China**

296 The rising levels of Asian aerosols could influence the meridional temperature and pressure  
297 gradients across the Indian Ocean and therefore affect monsoonal winds and rainfall in Australia  
298 since the middle of the 20<sup>th</sup> century, as reported in several previous studies (Fahrenbach et al.,  
299 2023; Rotstajn et al., 2007). Since 2013, aerosol levels in China have substantially decreased due



300 to clean air actions initiated by the Chinese government (Zhang et al., 2019). At the same time,  
301 precipitation in Australia exhibited a declining trend, which could be partly attributed to the  
302 decrease in China's anthropogenic aerosol forcing as quantified through CESM1 simulations.

303 Asian monsoon region is closely connected with the meridional Hadley circulation and zonal  
304 Walker circulation through monsoon outflow to the South India ocean subtropical high (SISH) and  
305 North Pacific subtropical high (NPSH) (Beck et al., 2018). Figure S16 illustrates the climatological  
306 mean wind fields at 850 hPa, indicating the persistent existence of SISH in the Indian Ocean and  
307 NPSH in the North Pacific. With reductions in aerosols in China, the sea surface temperature (SST)  
308 increases in the North Pacific but decreases in the Indian Ocean (Fig. S17), which is concurrent  
309 with the northward shift of the Intertropical Convergence Zone (ITCZ) (Basha et al., 2015). Over  
310 Asia, this migration of ITCZ is accompanied by the northward movement of the upper-  
311 tropospheric subtropical zonal westerly jet (Chiang et al., 2015; Schiemann et al., 2009), which  
312 moves to the north of the Tibetan Plateau. It then enhances the circulation pattern of the Tibetan  
313 high, redirects the outflow from the Asian monsoon to the southern Indian Ocean subtropical high  
314 (Fig. 3c), strengthens the SISH, and leads to the enhancement of the Southern Trade Winds (Fig.  
315 3d). On the other hand, the increase in SST in the North Pacific induces ascending motion around  
316 the 130°–150°E and the subsequent descending motion around the 90°–110°E (Fig. 3b), with  
317 anomalous westerly winds near the surface, leading to a weakening of NPSH along with a decrease  
318 in the Northern Trade Winds (Fig. 3d). Note that, the descending motion partly compensates the  
319 ascending motion related to the meridional circulation between 10°–30°N (Fig. 3c). Similar  
320 changes of vertical and horizontal circulations are also shown in the real world in the 2010s (Fig.  
321 S18). The enhancement of the Southern Trade Winds further causes moisture advection away from  
322 Australia, accompanied by moisture divergence in Australia, especially over the northern Australia  
323 (Fig. S19). Moisture divergence is also evident in the observations for some northern regions of  
324 Australia (Fig. S20). This moisture divergence in Australia then intensifies the dryness in Australia  
325 both in CESM1 simulations (Fig. 1) and ERA5 reanalysis (Fig. 2).

326 Figures S21 illustrate the changes in relevant radiative fluxes in Australia resulting from  
327 aerosol changes in China. Under the clear sky condition, both surface and top of the atmosphere  
328 (TOA) radiative flux decrease (Fig. S21c&d). It is due to increased sea salt and dust aerosols (Fig.  
329 S22b–d) due to the stronger Southern Trade Winds (Figs. S22a and 3d) and dryer conditions (Fig.



330 1a&c). The decrease in cloud cover (Fig. S12) leads to an overall increase in both surface and TOA  
331 radiative flux (Fig. S21e&f). The overall changes in radiative fluxes are offset by these two factors  
332 (Fig. S21a&b) and insufficient to explain the significant increase in surface air temperature in  
333 Australia (Fig. 1b). Similar signals are also evident in the observational data represented by ERA5  
334 and CERES-EBAF (Figs. S23 and S24).

335 Decreases in precipitation lead to a decrease in surface specific humidity (Fig. S25a), which  
336 declines more than that at 850 hPa (Fig. S25b). This results in excess energy being converted into  
337 sensible heat rather than latent heat through evaporation (Chiang et al., 2018; Fischer et al., 2007;  
338 Seneviratne et al., 2006; Su et al., 2014), which is indicated by a decrease in surface upward latent  
339 heat flux and an increase in surface upward sensible heat flux in Australia due to aerosol changes  
340 in China in Figure S26. The increased surface upward sensible heat flux heats the near-surface air  
341 and contributes to the warm conditions in Australia. The signals of specific humidity and surface  
342 sensible/latent heat flux from ERA5 are consistent with the simulated results. (Figs. S27 and S28).

### 343 **3.3 Increases in Wildfire Risk in Australia**

344 Wildfires represent a biosphere-atmosphere phenomenon, arising from the intricate interplay  
345 of weather, climate, fuels, and human activities (Moritz et al., 2014). Notably, wildfires are ranked  
346 among the most significant natural disasters in Australia, causing extensive damage (Shi et al.,  
347 2021). Collins et al. (2022) reported that warmer and drier conditions increased the potential for  
348 large and severe wildfire in Australia. Given that changes in aerosols in China have led to a warmer  
349 and drier climate condition in Australia in recent years, the change in this climate state could also  
350 impact on the occurrence of wildfires. Three wildfire risk indices ( $ET_0$ , VPD, and FFDI) are  
351 selected to assess the risks of wildfires occurrence. Detailed information about the three wildfire  
352 risk indices can be found in the Methods section.

353 All three indices exhibit increases ( $+0.36 \text{ mm mon}^{-1}$  for  $ET_0$ ,  $+0.56 \text{ hPa}$  for VPD, and  $+0.24$   
354 for FFDI) during fire seasons (September to February) in Australia due to changes in aerosols in  
355 China during 2013–2019 (Fig. 4), although they do not show the same spatial distribution possibly  
356 due to different considerations regarding climate variables in the indices. The results analyzed  
357 from observational data also exhibit increasing trends at a rate of  $0.32 \text{ mm mon}^{-1} \text{ yr}^{-1}$  for  $ET_0$ ,  $0.59$   
358  $\text{hPa yr}^{-1}$  for VPD, and  $0.34 \text{ yr}^{-1}$  for FFDI during this time period (Fig. S29). It further indicates



359 that the decline in anthropogenic aerosols in China can explain 12%–19% of the increase in  
360 wildfire risks during the fire season in Australia between 2013 and 2019 through inducing dry and  
361 warm wildfire weather conditions (Fig. S9).

#### 362 **4 Conclusions and Discussions**

363 This study reveals a plausible connection between the substantial aerosol reduction in China  
364 and drying and warming trends in Australia that happened during the 2010s. Aerosol reductions in  
365 China induce changes in temperature and pressure gradients, which lead to an increased outflow  
366 from Asia towards the South Indian Ocean, strengthening the SISH and the associated Southern  
367 Trade Winds. Consequently, this atmospheric pattern results in moisture divergence over Australia,  
368 causing a decrease in humidity and precipitation. The reduction in surface moisture leads to more  
369 surface energy being converted into sensible heat, rather than evaporating as latent heat, thereby  
370 heating the near-surface air. This perspective sheds light on the influence of distant aerosols on  
371 climate in Australia.

372 The CESM1 simulations depict warmer and drier conditions in Australia related to China's  
373 aerosol reductions than otherwise, a pattern also evident in observations represented by ERA5.  
374 However, it is important to note that China's aerosol reductions only contribute to a portion of the  
375 observed warm and dry conditions in Australia. According to the CESM1 simulations, aerosol  
376 changes in China account for 19% of the observed decrease in relative humidity and precipitation  
377 and 8% of the increase in temperature in Australia throughout the year, and 12%–19% of the  
378 increase in wildfire risks during the fire season in Australia during 2013–2019. Nonetheless, air  
379 quality and human health improvements owing to aerosol reductions cannot be ignored (Giani et  
380 al., 2020; Zheng et al., 2017). In addition, the drying and warming trends in Australia attributed to  
381 aerosol reductions should be considered resulting from the rise in long-lived GHGs, while the  
382 aerosol reductions unmask the effect rooted in the GHGs (Wang et al., 2023). In addition, other  
383 factors such as internal climate variability (Heidemann et al., 2023) appear to have contributed  
384 more to the changes in Australia's climate conditions.

385 There are some potential limitations and uncertainties in this study. Firstly, the low bias in  
386 simulated aerosol concentrations in CESM1 could potentially lead to an underestimation of the  
387 climate responses in Australia, and the extent to which the low bias could influence the results



388 remains unknown. Secondly, our findings are derived from simulations conducted with a single  
389 aerosol-climate model, and it is vital for future research to employ multi-model ensemble  
390 simulations to reduce the possibility of model-dependent specific results. While the CMIP6 and  
391 PDRMIP (Precipitation Driver Response Model Intercomparison Project) can assist in minimizing  
392 such model dependencies, they also present certain drawbacks. Anthropogenic emissions input in  
393 CMIP6 inadequately accounts for aerosol reductions resulting from clean air actions in China since  
394 2013 (Z. Wang et al., 2021). Additionally, CMIP6 considers aerosol changes globally, making it  
395 challenging to isolate effects specifically induced by changes in aerosols in China. The  
396 experimental design of PDRMIP, which scales the concentrations of sulfate and BC in Asia to ten  
397 times of their present-day levels, is generally idealistic and may not accurately and proportionally  
398 represent aerosol changes observed in the real world. Until now, few studies have explored the  
399 link between the recent reduction in China's aerosols and the changing climate conditions in  
400 Australia. Although Fahrenbach et al. (2023) investigated the connection between increased  
401 precipitation in Australia and elevated aerosol levels in Asia since the last century, they focused  
402 on the decadal time scale with historical increasing aerosols in Asia. Finally, in addition to aerosols,  
403 GHGs also contribute to regional and global climate change. The extent to which GHGs could  
404 contribute to weather condition and climate changes in Australia remains unknown, which  
405 warrants further investigation.

406 Nonetheless, our study examined the role of China's aerosol reductions in Australia's recent  
407 drying and warming trends. Substantial emission reductions will continue in China following the  
408 carbon neutral pathway (Yang et al., 2023), while future changes in emissions in South Asia remain  
409 uncertain (Samset et al., 2019). Apart from natural climate variabilities that affect the Australian  
410 monsoon, further investigation of changes in monsoon precipitation in Australia should also  
411 consider the effects of remote aerosol changes simultaneously, which is crucial to effective drought  
412 and wildfire management and mitigation in Australia.

#### 413 **Acknowledgments**

414 This study was supported by the National Natural Science Foundation of China (grant no.  
415 42475032), the Jiangsu Science Fund for Carbon Neutrality (grant no. BK20220031), and Jiangsu  
416 Innovation and Entrepreneurship Team (grant no. JSSCTD202346). H.W. acknowledges the



417 support of the U.S. Department of Energy (DOE), Office of Science, Office of Biological and  
418 Environmental Research (BER), as part of the Earth and Environmental System Modeling program.  
419 The Pacific Northwest National Laboratory (PNNL) is operated for DOE by the Battelle Memorial  
420 Institute under contract DE-AC05-76RLO1830.

#### 421 **Data and Code Availability**

422 Ground-based observed  $PM_{2.5}$  concentrations from CNEMC are available at  
423 <https://quotsoft.net/air/> (last access: September 2024). AOD from MODIS Deep Blue retrieval are  
424 available at <https://modis.gsfc.nasa.gov/> (last access: September 2024). ERA5 reanalysis data are  
425 available at <https://cds.climate.copernicus.eu/> (last access: September 2024). CERES-EBAF data  
426 are available at <https://ceres.larc.nasa.gov/data/#energy-balanced-and-filled-ebaf> (last access:  
427 September 2024). GPM data are available at  
428 [https://disc.gsfc.nasa.gov/datasets/GPM\\_3IMERGM\\_07/summary?keywords=%22IMERG%20fi  
429 nal%22](https://disc.gsfc.nasa.gov/datasets/GPM_3IMERGM_07/summary?keywords=%22IMERG%20final%22) (last access: September 2024). The source code of CESM is available at  
430 <https://github.com/ESCOMP/CESM> (last access: September 2024). Our model results can be  
431 available at <https://doi.org/10.5281/zenodo.13682943> (last access: September 2024).

#### 432 **Author Contributions**

433 Y.Y. conceived the research and directed the analysis. J.G. conceived the research, conducted  
434 the model simulations, and performed the analysis. All the authors including H.W., P.W., and H.  
435 L. discussed the results and wrote the paper.

#### 436 **Competing Interests**

437 At least one of the (co-)authors is a member of the editorial board of Atmospheric Chemistry  
438 and Physics.

#### 439 **References**

440 Basha, G., Kishore, P., Venkat Ratnam, M., Ouarda, T. B. M. J., Velicogna, I., and Sutterley, T.:  
441 Vertical and latitudinal variation of the intertropical convergence zone derived using GPS  
442 radio occultation measurements, *Remote Sens. Environ.*, 163, 262–269,  
443 <https://doi.org/10.1016/j.rse.2015.03.024>, 2015.





- 444 Beck, J. W., Zhou, W., Li, C., Wu, Z., White, L., Xian, F., Kong, X., and An, Z.: A 550,000-year  
445 record of East Asian monsoon rainfall from 10Be in loess, *Science*, 360, 877–881,  
446 <https://doi.org/10.1126/science.aam5825>, 2018.
- 447 Boer, M. M., Resco De Dios, V., and Bradstock, R. A.: Unprecedented burn area of Australian  
448 mega forest fires, *Nat. Clim. Change*, 10, 171–172, <https://doi.org/10.1038/s41558-020-0716-1>, 2020.
- 450 Bollasina, M. A., Ming, Y., and Ramaswamy, V.: Anthropogenic Aerosols and the Weakening of  
451 the South Asian Summer Monsoon, *Science*, 334, 502–505,  
452 <https://doi.org/10.1126/science.1204994>, 2011.
- 453 Bollasina, M. A., Ming, Y., Ramaswamy, V., Schwarzkopf, M. D., and Naik, V.: Contribution of  
454 local and remote anthropogenic aerosols to the twentieth century weakening of the South  
455 Asian Monsoon, *Geophys. Res. Lett.*, 41, 680–687, <https://doi.org/10.1002/2013GL058183>,  
456 2014.
- 457 Chiang, F., Mazdiyasi, O., and AghaKouchak, A.: Amplified warming of droughts in southern  
458 United States in observations and model simulations, *Sci. Adv.*, 4, eaat2380,  
459 <https://doi.org/10.1126/sciadv.aat2380>, 2018.
- 460 Chiang, J. C. H., Fung, I. Y., Wu, C.-H., Cai, Y., Edman, J. P., Liu, Y., Day, J. A., Bhattacharya,  
461 T., Mondal, Y., and Labrousse, C. A.: Role of seasonal transitions and westerly jets in East  
462 Asian paleoclimate, *Quat. Sci. Rev.*, 108, 111–129,  
463 <https://doi.org/10.1016/j.quascirev.2014.11.009>, 2015.
- 464 Collins, L., Clarke, H., Clarke, M. F., McColl Gausden, S. C., Nolan, R. H., Penman, T., and  
465 Bradstock, R.: Warmer and drier conditions have increased the potential for large and severe  
466 fire seasons across south-eastern Australia, *Glob. Ecol. Biogeogr.*, 31, 1933–1948,  
467 <https://doi.org/10.1111/geb.13514>, 2022.
- 468 Cook, B. I. and Seager, R.: The response of the North American Monsoon to increased greenhouse  
469 gas forcing, *J. Geophys. Res.: Atmos.*, 118, 1690–1699, <https://doi.org/10.1002/jgrd.50111>,  
470 2013.
- 471 Cowan, T. and Cai, W.: The impact of Asian and non-Asian anthropogenic aerosols on 20th  
472 century Asian summer monsoon: ASIAN MONSOON AND AEROSOLS, *Geophys. Res.  
473 Lett.*, 38, L11703, <https://doi.org/10.1029/2011GL047268>, 2011.
- 474 CSIRO and BOM: State of the Climate 2022, 2022
- 475 Dang, R. and Liao, H.: Radiative Forcing and Health Impact of Aerosols and Ozone in China as  
476 the Consequence of Clean Air Actions over 2012–2017, *Geophys. Res. Lett.*, 46, 12511–  
477 12519, <https://doi.org/10.1029/2019GL084605>, 2019.
- 478 Dey, R., Lewis, S. C., Arblaster, J. M., and Abram, N. J.: A review of past and projected changes  
479 in Australia’s rainfall, *WIREs Clim. Change*, 10, e577, <https://doi.org/10.1002/wcc.577>,  
480 2019a.



- 481 Dey, R., Lewis, S. C., and Abram, N. J.: Investigating observed northwest Australian rainfall  
482 trends in Coupled Model Intercomparison Project phase 5 detection and attribution  
483 experiments, *Int. J. Climatol.*, 39, 112–127, <https://doi.org/10.1002/joc.5788>, 2019b.
- 484 Dong, B., Wilcox, L. J., Highwood, E. J., and Sutton, R. T.: Impacts of recent decadal changes in  
485 Asian aerosols on the East Asian summer monsoon: roles of aerosol–radiation and aerosol–  
486 cloud interactions, *Clim. Dyn.*, 53, 3235–3256, <https://doi.org/10.1007/s00382-019-04698-0>,  
487 2019.  
488
- 489 Dowdy, A. J.: Seamless climate change projections and seasonal predictions for bushfires in  
490 Australia, *J. South. Hemisph. Earth Syst. Sci.*, 70, 120–138, <https://doi.org/10.1071/ES20001>,  
491 2020.
- 492 Evans, S., Marchand, R., and Ackerman, T.: Variability of the Australian Monsoon and  
493 Precipitation Trends at Darwin, *J. Climate*, 27, 8487–8500, <https://doi.org/10.1175/JCLI-D-13-00422.1>, 2014.  
494
- 495 Fahrenbach, N. L. S., Bollasina, M. A., Samset, B. H., Cowan, T., and Ekman, A. M. L.: Asian  
496 anthropogenic aerosol forcing played a key role in the multi-decadal increase in Australian  
497 summer monsoon rainfall, *J. Climate*, 1, <https://doi.org/10.1175/JCLI-D-23-0313.1>, 2023.
- 498 Fan, T., Liu, X., Ma, P.-L., Zhang, Q., Li, Z., Jiang, Y., Zhang, F., Zhao, C., Yang, X., Wu, F., and  
499 Wang, Y.: Emission or atmospheric processes? An attempt to attribute the source of large  
500 bias of aerosols in eastern China simulated by global climate models, *Atmos. Chem. Phys.*,  
501 18, 1395–1417, <https://doi.org/10.5194/acp-18-1395-2018>, 2018.
- 502 Fan, T., Liu, X., Wu, C., Zhang, Q., Zhao, C., Yang, X., and Li, Y.: Comparison of the  
503 Anthropogenic Emission Inventory for CMIP6 Models with a Country-Level Inventory over  
504 China and the Simulations of the Aerosol Properties, *Adv. Atmos. Sci.*, 39, 80–96,  
505 <https://doi.org/10.1007/s00376-021-1119-6>, 2022.
- 506 Fischer, E. M., Seneviratne, S. I., Lüthi, D., and Schär, C.: Contribution of land-atmosphere  
507 coupling to recent European summer heat waves, *Geophys. Res. Lett.*, 34, 2006GL029068,  
508 <https://doi.org/10.1029/2006GL029068>, 2007.
- 509 Gao, J., Yang, Y., Wang, H., Wang, P., Li, H., Li, M., Ren, L., Yue, X., and Liao, H.: Fast climate  
510 responses to emission reductions in aerosol and ozone precursors in China during 2013–2017,  
511 *Atmos. Chem. Phys.*, 22, 7131–7142, <https://doi.org/10.5194/acp-22-7131-2022>, 2022.
- 512 Gao, J., Yang, Y., Wang, H., Wang, P., Li, B., Li, J., Wei, J., Gao, M., and Liao, H.: Climate  
513 responses in China to domestic and foreign aerosol changes due to clean air actions during  
514 2013–2019, *npj Clim. Atmos. Sci.*, 6, 160, <https://doi.org/10.1038/s41612-023-00488-y>,  
515 2023.
- 516 Giani, P., Castruccio, S., Anav, A., Howard, D., Hu, W., and Crippa, P.: Short-term and long-term  
517 health impacts of air pollution reductions from COVID-19 lockdowns in China and Europe:



- 518 a modelling study, *Lancet Planet. Health*, 4, e474–e482, [https://doi.org/10.1016/S2542-5196\(20\)30224-2](https://doi.org/10.1016/S2542-5196(20)30224-2), 2020.
- 519
- 520 Guenther, A. B., Jiang, X., Heald, C. L., Sakulyanontvittaya, T., Duhl, T., Emmons, L. K., and  
521 Wang, X.: The Model of Emissions of Gases and Aerosols from Nature version 2.1  
522 (MEGAN2.1): an extended and updated framework for modeling biogenic emissions, *Geosci.  
523 Model Dev.*, 5, 1471–1492, <https://doi.org/10.5194/gmd-5-1471-2012>, 2012.
- 524 He, T., Lamont, B. B., and Pausas, J. G.: Fire as a key driver of Earth’s biodiversity, *Biol. Rev.*,  
525 94, 1983–2010, <https://doi.org/10.1111/brv.12544>, 2019.
- 526 Head, L., Adams, M., McGregor, H. V., and Toole, S.: Climate change and Australia, *WIREs Clim.  
527 Change*, 5, 175–197, <https://doi.org/10.1002/wcc.255>, 2014.
- 528 Heidemann, H., Cowan, T., Henley, B. J., Ribbe, J., Freund, M., and Power, S.: Variability and  
529 long-term change in Australian monsoon rainfall: A review, *WIREs Clim. Change*, 14, e823,  
530 <https://doi.org/10.1002/wcc.823>, 2023.
- 531 Hersbach, H., Bell, B., Berrisford, P., Hirahara, S., Horányi, A., Muñoz-Sabater, J., Nicolas, J.,  
532 Peubey, C., Radu, R., Schepers, D., Simmons, A., Soci, C., Abdalla, S., Abellan, X., Balsamo,  
533 G., Bechtold, P., Biavati, G., Bidlot, J., Bonavita, M., De Chiara, G., Dahlgren, P., Dee, D.,  
534 Diamantakis, M., Dragani, R., Flemming, J., Forbes, R., Fuentes, M., Geer, A., Haimberger,  
535 L., Healy, S., Hogan, R. J., Hólm, E., Janisková, M., Keeley, S., Laloyaux, P., Lopez, P.,  
536 Lupu, C., Radnoti, G., De Rosnay, P., Rozum, I., Vamborg, F., Villaume, S., and Thépaut, J.:  
537 The ERA5 global reanalysis, *Q. J. R. Meteorol. Soc.*, 146, 1999–2049,  
538 <https://doi.org/10.1002/qj.3803>, 2020.
- 539 Hoesly, R. M., Smith, S. J., Feng, L., Klimont, Z., Janssens-Maenhout, G., Pitkanen, T., Seibert,  
540 J. J., Vu, L., Andres, R. J., Bolt, R. M., Bond, T. C., Dawidowski, L., Kholod, N., Kurokawa,  
541 J., Li, M., Liu, L., Lu, Z., Moura, M. C. P., O’Rourke, P. R., and Zhang, Q.: Historical (1750–  
542 2014) anthropogenic emissions of reactive gases and aerosols from the Community Emissions  
543 Data System (CEDS), *Geosci. Model Dev.*, 11, 369–408, <https://doi.org/10.5194/gmd-11-369-2018>, 2018.
- 544
- 545 Hsu, N. C., Jeong, M. -J., Bettenhausen, C., Sayer, A. M., Hansell, R., Seftor, C. S., Huang, J., and  
546 Tsay, S. -C.: Enhanced Deep Blue aerosol retrieval algorithm: The second generation, *J.  
547 Geophys. Res.: Atmos.*, 118, 9296–9315, <https://doi.org/10.1002/jgrd.50712>, 2013.
- 548 Huneeus, N., Denier Van Der Gon, H., Castesana, P., Menares, C., Granier, C., Granier, L., Alonso,  
549 M., De Fatima Andrade, M., Dawidowski, L., Gallardo, L., Gomez, D., Klimont, Z., Janssens-  
550 Maenhout, G., Osses, M., Puliafito, S. E., Rojas, N., Ccoyllo, O. S., Tolvett, S., and Ynoue,  
551 R. Y.: Evaluation of anthropogenic air pollutant emission inventories for South America at  
552 national and city scale, *Atmos. Environ.*, 235, 117606,  
553 <https://doi.org/10.1016/j.atmosenv.2020.117606>, 2020.
- 554 IPCC: Climate Change 2013: The Physical Science Basis, 2013.
- 555 IPCC: Climate Change 2021: The Physical Science Basis, 2021.



- 556 Irmak, S., Irmak, A., Allen, R. G., and Jones, J. W.: Solar and Net Radiation-Based Equations to  
557 Estimate Reference Evapotranspiration in Humid Climates, *J. Irrig. Drain. Eng.*, 129, 336–  
558 347, [https://doi.org/10.1061/\(ASCE\)0733-9437\(2003\)129:5\(336\)](https://doi.org/10.1061/(ASCE)0733-9437(2003)129:5(336)), 2003.
- 559 Johnston, F. H., Borchers-Arriagada, N., Morgan, G. G., Jalaludin, B., Palmer, A. J., Williamson,  
560 G. J., and Bowman, D. M. J. S.: Unprecedented health costs of smoke-related PM<sub>2.5</sub> from  
561 the 2019–20 Australian megafires, *Nat. Sustain.*, 4, 42–47, <https://doi.org/10.1038/s41893-020-00610-5>, 2021.
- 563 Jones, M. W., Abatzoglou, J. T., Veraverbeke, S., Andela, N., Lasslop, G., Forkel, M., Smith, A.  
564 J. P., Burton, C., Betts, R. A., van der Werf, G. R., Sitch, S., Canadell, J. G., Santín, C.,  
565 Kolden, C., Doerr, S. H., and Le Quéré, C.: Global and Regional Trends and Drivers of Fire  
566 Under Climate Change, *Rev. Geophys.*, 60, e2020RG000726, <https://doi.org/10.1029/2020RG000726>, 2022.
- 568 Kloster, S., Dentener, F., Feichter, J., Raes, F., Lohmann, U., Roeckner, E., and Fischer-Bruns, I.:  
569 A GCM study of future climate response to aerosol pollution reductions, *Clim. Dyn.*, 34,  
570 1177–1194, <https://doi.org/10.1007/s00382-009-0573-0>, 2010.
- 571 Lau, K.-M. and Kim, K.-M.: Observational relationships between aerosol and Asian monsoon  
572 rainfall, and circulation, *Geophys. Res. Lett.*, 33, 2006GL027546, <https://doi.org/10.1029/2006GL027546>, 2006.
- 574 Leibensperger, E. M., Mickley, L. J., Jacob, D. J., Chen, W.-T., Seinfeld, J. H., Nenes, A., Adams,  
575 P. J., Streets, D. G., Kumar, N., and Rind, D.: Climatic effects of 1950–2050 changes in US  
576 anthropogenic aerosols – Part 1: Aerosol trends and radiative forcing, *Atmos. Chem. Phys.*,  
577 12, 3333–3348, <https://doi.org/10.5194/acp-12-3333-2012>, 2012.
- 578 Liu, C., Yang, Y., Wang, H., Ren, L., Wei, J., Wang, P., and Liao, H.: Influence of Spatial Dipole  
579 Pattern in Asian Aerosol Changes on East Asian Summer Monsoon, *J. Climate*, 36, 1575–  
580 1585, <https://doi.org/10.1175/JCLI-D-22-0335.1>, 2023.
- 581 Liu, X., Ma, P.-L., Wang, H., Tilmes, S., Singh, B., Easter, R. C., Ghan, S. J., and Rasch, P. J.:  
582 Description and evaluation of a new four-mode version of the Modal Aerosol Module  
583 (MAM4) within version 5.3 of the Community Atmosphere Model, *Geosci. Model Dev.*, 9,  
584 505–522, <https://doi.org/10.5194/gmd-9-505-2016>, 2016.
- 585 Loeb, N. G., Doelling, D. R., Wang, H., Su, W., Nguyen, C., Corbett, J. G., Liang, L., Mitrescu,  
586 C., Rose, F. G., and Kato, S.: Clouds and the Earth’s Radiant Energy System (CERES) Energy  
587 Balanced and Filled (EBAF) Top-of-Atmosphere (TOA) Edition-4.0 Data Product, *J. Climate*,  
588 31, 895–918, <https://doi.org/10.1175/JCLI-D-17-0208.1>, 2018.
- 589 Ming, Y. and Ramaswamy, V.: Nonlinear Climate and Hydrological Responses to Aerosol Effects,  
590 *J. Climate*, 22, 1329–1339, <https://doi.org/10.1175/2008JCLI2362.1>, 2009.
- 591 Moritz, M. A., Batllori, E., Bradstock, R. A., Gill, A. M., Handmer, J., Hessburg, P. F., Leonard,  
592 J., McCaffrey, S., Odion, D. C., Schoennagel, T., and Syphard, A. D.: Learning to coexist  
593 with wildfire, *Nature*, 515, 58–66, <https://doi.org/10.1038/nature13946>, 2014.



- 594 Nicholls, N.: Detecting and attributing Australian climate change: a review, *Aust. Meteorol. Mag.*,  
595 2006.
- 596 Oh, H. and Ha, K.-J.: Thermodynamic characteristics and responses to ENSO of dominant  
597 intraseasonal modes in the East Asian summer monsoon, *Clim. Dyn.*, 44, 1751–1766,  
598 <https://doi.org/10.1007/s00382-014-2268-4>, 2015.
- 599 Pozzoli, L., Janssens-Maenhout, G., Diehl, T., Bey, I., Schultz, M. G., Feichter, J., Vignati, E., and  
600 Dentener, F.: Re-analysis of tropospheric sulfate aerosol and ozone for the period 1980–2005  
601 using the aerosol-chemistry-climate model ECHAM5-HAMMOZ, *Atmos. Chem. Phys.*, 11,  
602 9563–9594, <https://doi.org/10.5194/acp-11-9563-2011>, 2011.
- 603 Rauniyar, S. P. and Power, S. B.: The Impact of Anthropogenic Forcing and Natural Processes on  
604 Past, Present, and Future Rainfall over Victoria, Australia, *J. Climate*, 33, 8087–8106,  
605 <https://doi.org/10.1175/JCLI-D-19-0759.1>, 2020.
- 606 Ren, L., Yang, Y., Wang, H., Wang, P., Yue, X., and Liao, H.: Widespread Wildfires Over the  
607 Western United States in 2020 Linked to Emissions Reductions During COVID-19, *Geophys.*  
608 *Res. Lett.*, 49, e2022GL099308, <https://doi.org/10.1029/2022GL099308>, 2022.
- 609 Risbey, J. S., Pook, M. J., McIntosh, P. C., Wheeler, M. C., and Hendon, H. H.: On the Remote  
610 Drivers of Rainfall Variability in Australia, *Mon. Wea. Rev.*, 137, 3233–3253,  
611 <https://doi.org/10.1175/2009MWR2861.1>, 2009.
- 612 Rotstayn, L. D., Cai, W., Dix, M. R., Farquhar, G. D., Feng, Y., Ginoux, P., Herzog, M., Ito, A.,  
613 Penner, J. E., Roderick, M. L., and Wang, M.: Have Australian rainfall and cloudiness  
614 increased due to the remote effects of Asian anthropogenic aerosols?, *J. Geophys. Res.:*  
615 *Atmos.*, 112, 2006JD007712, <https://doi.org/10.1029/2006JD007712>, 2007.
- 616 Samset, B. H., Lund, M. T., Bollasina, M., Myhre, G., and Wilcox, L.: Emerging Asian aerosol  
617 patterns, *Nat. Geosci.*, 12, 582–584, <https://doi.org/10.1038/s41561-019-0424-5>, 2019.
- 618 Schiemann, R., Lüthi, D., and Schär, C.: Seasonality and Interannual Variability of the Westerly  
619 Jet in the Tibetan Plateau Region, *J. Climate*, 22, 2940–2957,  
620 <https://doi.org/10.1175/2008JCLI2625.1>, 2009.
- 621 Seager, R., Hooks, A., Williams, A. P., Cook, B., Nakamura, J., and Henderson, N.: Climatology,  
622 Variability, and Trends in the U.S. Vapor Pressure Deficit, an Important Fire-Related  
623 Meteorological Quantity, *J. Appl. Meteorol. Clim.*, 54, 1121–1141,  
624 <https://doi.org/10.1175/JAMC-D-14-0321.1>, 2015.
- 625 Seneviratne, S. I., Lüthi, D., Litschi, M., and Schär, C.: Land–atmosphere coupling and climate  
626 change in Europe, *Nature*, 443, 205–209, <https://doi.org/10.1038/nature05095>, 2006.
- 627 Sharples, J. J., McRae, R. H. D., Weber, R. O., and Gill, A. M.: A simple index for assessing fire  
628 danger rating, *Environ. Modell. Softw.*, 24, 764–774,  
629 <https://doi.org/10.1016/j.envsoft.2008.11.004>, 2009.



- 630 Shi, G., Yan, H., Zhang, W., Dodson, J., Heijnis, H., and Burrows, M.: Rapid warming has resulted  
631 in more wildfires in northeastern Australia, *Sci. Total Environ.*, 771, 144888,  
632 <https://doi.org/10.1016/j.scitotenv.2020.144888>, 2021.
- 633 Skofronick-Jackson, G., Petersen, W. A., Berg, W., Kidd, C., Stocker, E. F., Kirschbaum, D. B.,  
634 Kakar, R., Braun, S. A., Huffman, G. J., Iguchi, T., Kirstetter, P. E., Kummerow, C.,  
635 Meneghini, R., Oki, R., Olson, W. S., Takayabu, Y. N., Furukawa, K., and Wilheit, T.: The  
636 Global Precipitation Measurement (GPM) Mission for Science and Society, *Bull. Am.*  
637 *Meteorol. Soc.*, 98, 1679–1695, <https://doi.org/10.1175/BAMS-D-15-00306.1>, 2017.
- 638 Streets, D. G., Yan, F., Chin, M., Diehl, T., Mahowald, N., Schultz, M., Wild, M., Wu, Y., and Yu,  
639 C.: Anthropogenic and natural contributions to regional trends in aerosol optical depth, 1980–  
640 2006, *J. Geophys. Res.: Atmos.*, 114, 2008JD011624, <https://doi.org/10.1029/2008JD011624>,  
641 2009.
- 642 Su, H., Yang, Z., Dickinson, R. E., and Wei, J.: Spring soil moisture-precipitation feedback in the  
643 Southern Great Plains: How is it related to large-scale atmospheric conditions?, *Geophys.*  
644 *Res. Lett.*, 41, 1283–1289, <https://doi.org/10.1002/2013GL058931>, 2014.
- 645 Turnock, S. T., Allen, R. J., Andrews, M., Bauer, S. E., Deushi, M., Emmons, L., Good, P.,  
646 Horowitz, L., John, J. G., Michou, M., Nabat, P., Naik, V., Neubauer, D., O'Connor, F. M.,  
647 Olivie, D., Oshima, N., Schulz, M., Sellar, A., Shim, S., Takemura, T., Tilmes, S., Tsigaridis,  
648 K., Wu, T., and Zhang, J.: Historical and future changes in air pollutants from CMIP6 models,  
649 *Atmos. Chem. Phys.*, 20, 14547–14579, <https://doi.org/10.5194/acp-20-14547-2020>, 2020.
- 650 Undorf, S., Polson, D., Bollasina, M. A., Ming, Y., Schurer, A., and Hegerl, G. C.: Detectable  
651 Impact of Local and Remote Anthropogenic Aerosols on the 20th Century Changes of West  
652 African and South Asian Monsoon Precipitation, *J. Geophys. Res.: Atmos.*, 123, 4871–4889,  
653 <https://doi.org/10.1029/2017JD027711>, 2018.
- 654 Van Marle, M. J. E., Kloster, S., Magi, B. I., Marlon, J. R., Daniau, A.-L., Field, R. D., Arneth, A.,  
655 Forrest, M., Hantson, S., Kehrwald, N. M., Knorr, W., Lasslop, G., Li, F., Mangeon, S., Yue,  
656 C., Kaiser, J. W., and Van Der Werf, G. R.: Historic global biomass burning emissions for  
657 CMIP6 (BB4CMIP) based on merging satellite observations with proxies and fire models  
658 (1750–2015), *Geosci. Model Dev.*, 10, 3329–3357, [https://doi.org/10.5194/gmd-10-3329-](https://doi.org/10.5194/gmd-10-3329-2017)  
659 2017, 2017.
- 660 Wang, B., Biasutti, M., Byrne, M. P., Castro, C., Chang, C.-P., Cook, K., Fu, R., Grimm, A. M.,  
661 Ha, K.-J., Hendon, H., Kitoh, A., Krishnan, R., Lee, J.-Y., Li, J., Liu, J., Moise, A., Pascale,  
662 S., Roxy, M. K., Seth, A., Sui, C.-H., Turner, A., Yang, S., Yun, K.-S., Zhang, L., and Zhou,  
663 T.: Monsoons Climate Change Assessment, *Bull. Am. Meteorol. Soc.*, 102, E1–E19,  
664 <https://doi.org/10.1175/BAMS-D-19-0335.1>, 2021.
- 665 Wang, H., Easter, R. C., Rasch, P. J., Wang, M., Liu, X., Ghan, S. J., Qian, Y., Yoon, J.-H., Ma,  
666 P.-L., and Vinoj, V.: Sensitivity of remote aerosol distributions to representation of cloud–  
667 aerosol interactions in a global climate model, *Geosci. Model Dev.*, 6, 765–782,  
668 <https://doi.org/10.5194/gmd-6-765-2013>, 2013.



- 669 Wang, P., Yang, Y., Xue, D., Ren, L., Tang, J., Leung, L. R., and Liao, H.: Aerosols overtake  
670 greenhouse gases causing a warmer climate and more weather extremes toward carbon  
671 neutrality, *Nat. Commun.*, 14, 7257, <https://doi.org/10.1038/s41467-023-42891-2>, 2023.
- 672 Wang, Z., Zhang, H., and Zhang, X.: Projected response of East Asian summer monsoon system  
673 to future reductions in emissions of anthropogenic aerosols and their precursors, *Clim. Dyn.*,  
674 47, 1455–1468, <https://doi.org/10.1007/s00382-015-2912-7>, 2016.
- 675 Wang, Z., Lin, L., Xu, Y., Che, H., Zhang, X., Zhang, H., Dong, W., Wang, C., Gui, K., and Xie,  
676 B.: Incorrect Asian aerosols affecting the attribution and projection of regional climate change  
677 in CMIP6 models, *npj Clim. Atmos. Sci.*, 4, 2, <https://doi.org/10.1038/s41612-020-00159-2>,  
678 2021.
- 679 Ward, M., Tulloch, A. I. T., Radford, J. Q., Williams, B. A., Reside, A. E., Macdonald, S. L.,  
680 Mayfield, H. J., Maron, M., Possingham, H. P., Vine, S. J., O’Connor, J. L., Massingham, E.  
681 J., Greenville, A. C., Woinarski, J. C. Z., Garnett, S. T., Lintermans, M., Scheele, B. C.,  
682 Carwardine, J., Nimmo, D. G., Lindenmayer, D. B., Kooyman, R. M., Simmonds, J. S., Sonter,  
683 L. J., and Watson, J. E. M.: Impact of 2019–2020 mega-fires on Australian fauna habitat, *Nat.*  
684 *Ecol. Evol.*, 4, 1321–1326, <https://doi.org/10.1038/s41559-020-1251-1>, 2020.
- 685 Wasko, C., Shao, Y., Vogel, E., Wilson, L., Wang, Q. J., Frost, A., and Donnelly, C.:  
686 Understanding trends in hydrologic extremes across Australia, *J. Hydrol.*, 593, 125877,  
687 <https://doi.org/10.1016/j.jhydrol.2020.125877>, 2021.
- 688 Yang, Y., Zeng, L., Wang, H., Wang, P., and Liao, H.: Climate effects of future aerosol reductions  
689 for achieving carbon neutrality in China, *Sci. Bull.*, 68, 902–905,  
690 <https://doi.org/10.1016/j.scib.2023.03.048>, 2023.
- 691 Zacharakis, I. and Tsihrintzis, V. A.: Integrated wildfire danger models and factors: A review, *Sci.*  
692 *Total Environ.*, 899, 165704, <https://doi.org/10.1016/j.scitotenv.2023.165704>, 2023.
- 693 Zeng, L., Yang, Y., Wang, H., Wang, J., Li, J., Ren, L., Li, H., Zhou, Y., Wang, P., and Liao, H.:  
694 Intensified modulation of winter aerosol pollution in China by El Niño with short duration,  
695 *Atmos. Chem. Phys.*, 21, 10745–10761, <https://doi.org/10.5194/acp-21-10745-2021>, 2021.
- 696 Zhang, Q., Zheng, Y., Tong, D., Shao, M., Wang, S., Zhang, Y., Xu, X., Wang, J., He, H., Liu,  
697 W., Ding, Y., Lei, Y., Li, J., Wang, Z., Zhang, X., Wang, Y., Cheng, J., Liu, Y., Shi, Q., Yan,  
698 L., Geng, G., Hong, C., Li, M., Liu, F., Zheng, B., Cao, J., Ding, A., Gao, J., Fu, Q., Huo, J.,  
699 Liu, B., Liu, Z., Yang, F., He, K., and Hao, J.: Drivers of improved PM<sub>2.5</sub> air quality in China  
700 from 2013 to 2017, *Proc. Natl. Acad. Sci.*, 116, 24463–24469,  
701 <https://doi.org/10.1073/pnas.1907956116>, 2019.
- 702 Zheng, B., Tong, D., Li, M., Liu, F., Hong, C., Geng, G., Li, H., Li, X., Peng, L., Qi, J., Yan, L.,  
703 Zhang, Y., Zhao, H., Zheng, Y., He, K., and Zhang, Q.: Trends in China’s anthropogenic  
704 emissions since 2010 as the consequence of clean air actions, *Atmos. Chem. Phys.*, 18,  
705 14095–14111, <https://doi.org/10.5194/acp-18-14095-2018>, 2018.

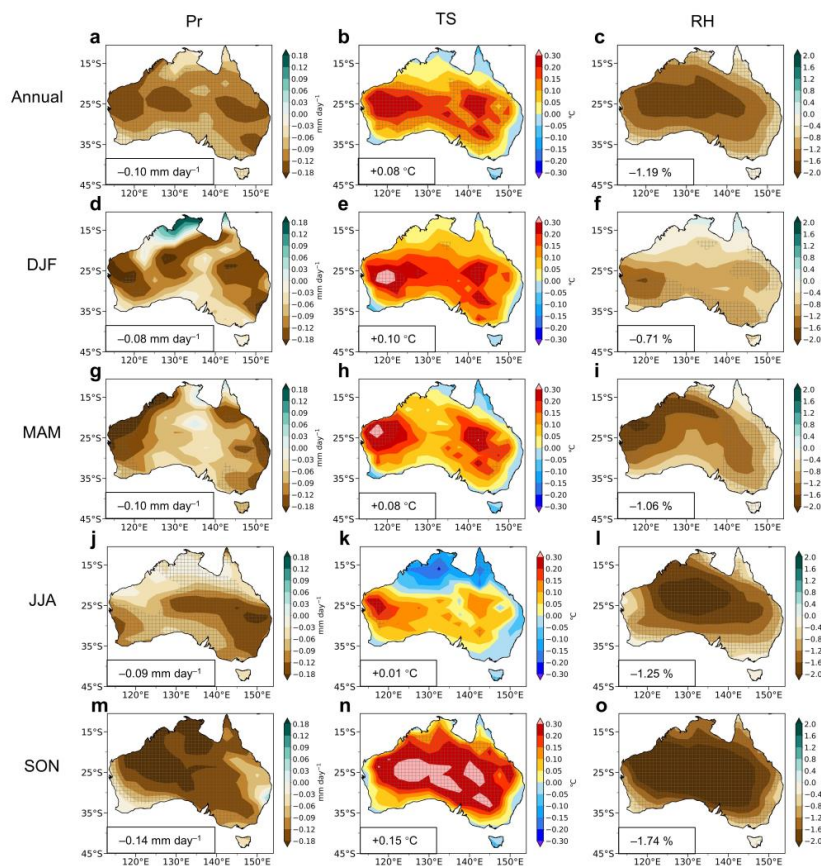


706 Zheng, Y., Xue, T., Zhang, Q., Geng, G., Tong, D., Li, X., and He, K.: Air quality improvements  
707 and health benefits from China's clean air action since 2013, *Environ. Res. Lett.*, 12, 114020,  
708 <https://doi.org/10.1088/1748-9326/aa8a32>, 2017.

709 Zheng, Y., Zhang, Q., Tong, D., Davis, S. J., and Caldeira, K.: Climate effects of China's efforts  
710 to improve its air quality, *Environ. Res. Lett.*, 15, 104052, [https://doi.org/10.1088/1748-](https://doi.org/10.1088/1748-9326/ab9e21)  
711 [9326/ab9e21](https://doi.org/10.1088/1748-9326/ab9e21), 2020.

712

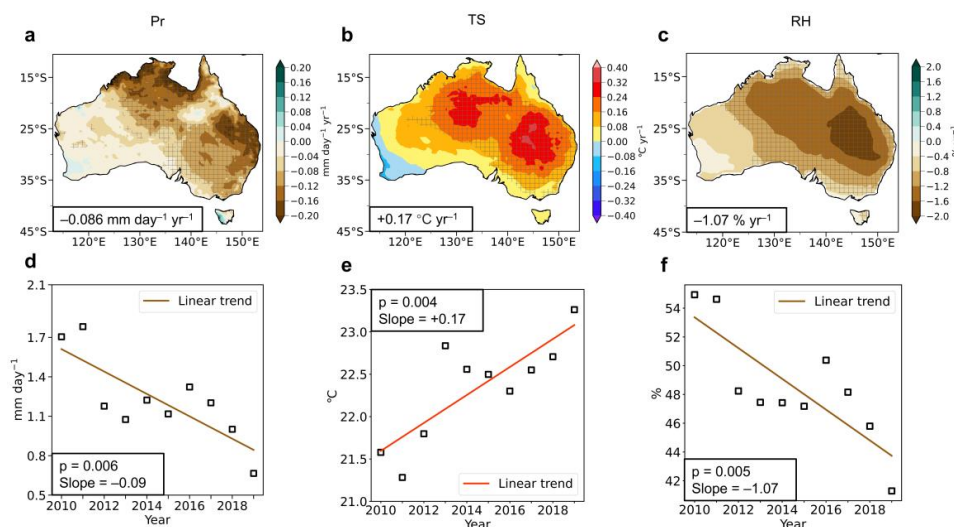




713

714 **Figure 1. Simulated changes in precipitation rate, surface air temperature and relative**  
 715 **humidity in Australia due to aerosol changes in China between 2013 and 2019. Spatial**  
 716 **distributions of simulated differences in annual (a–c), DJF (d–f, December, January and February),**  
 717 **MAM (g–I, March, April and May), JJA (j–l, June, July and August) and SON (m–o, September,**  
 718 **October and November) mean precipitation rate (Pr, a, d, g, j, and m, unit: mm day<sup>-1</sup>), surface air**  
 719 **temperature (TS, b, e, h, k, and n, unit: °C) and relative humidity (RH, c, f, i, l, and o, unit: %) in**  
 720 **Australia between BASE and CHN (CHN minus BASE). The shaded areas indicate results are**  
 721 **statistically significant at the 90% confidence level. Regional averages over Australia are noted at**  
 722 **the bottom-left corner of each panel.**

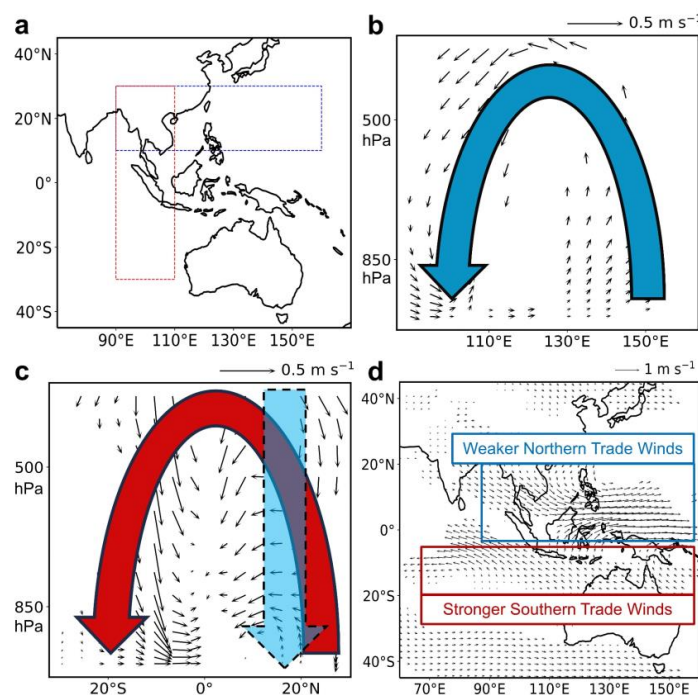
723



724

725 **Figure 2. Linear trends of observed precipitation rate, surface air temperature and relative**  
726 **humidity in Australia based on ERA5.** Spatial distributions of linear trends (a, b, and c) and  
727 time series (d, e, and f) of annual mean precipitation rate (Pr, a and d, unit:  $\text{mm day}^{-1}$ ), surface air  
728 temperature (TS, b and e, unit:  $^{\circ}\text{C}$ ) and relative humidity (RH, c and f, unit:  $\%$ ) in Australia during  
729 2010–2019 from ERA5 reanalysis. The shaded areas indicate trends are statistically significant at  
730 the 90% confidence level. Regional averages over Australia are noted at the bottom-left corner of  
731 panels a, b, and c. The p values and slopes of linear trends are noted in panels d, e, and f.

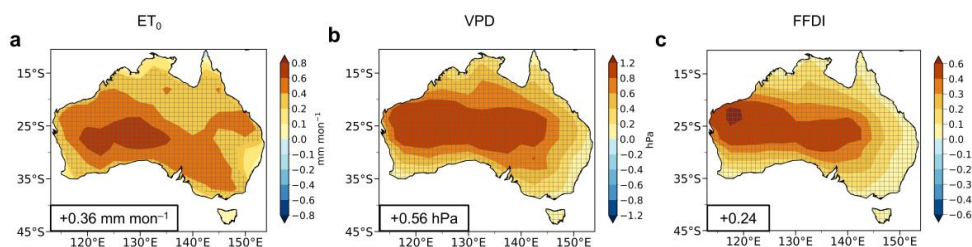
732



733

734 **Figure 3. Simulated changes in vertical circulations and 850 hPa wind fields in Asia-Pacific**  
735 **regions due to aerosol changes in China between 2013 and 2019.** Panel b and c shows pressure–  
736 longitude and pressure–latitude cross-section of responses in annual mean atmospheric  
737 circulations (unit:  $\text{m s}^{-1}$ , vectors), respectively, over the areas marked with the blue and red box in  
738 panel a. Panel d shows annual mean changes in wind fields (unit:  $\text{m s}^{-1}$ , vectors) at 850 hPa in  
739 Asia-Pacific regions. Only atmospheric circulations and winds statistically significant at the 90%  
740 confidence level are shown.

741



742

743 **Figure 4. Simulated changes in reference potential evapotranspiration, vapor pressure**  
744 **deficit, and McArthur forest fire danger index during fire seasons in Australia due to aerosol**  
745 **changes in China between 2013 and 2019.** Spatial distributions of simulated changes in reference  
746 potential evapotranspiration ( $ET_0$ , **a**, unit:  $\text{mm mon}^{-1}$ ), vapor pressure deficit (VPD, **b**, unit: hPa),  
747 and McArthur forest fire danger index (FFDI, **c**, unitless) during fire seasons (austral spring and  
748 summer, from September to the February of the next year) in Australia between BASE and CHN  
749 (CHN minus BASE). The shaded areas indicate results are statistically significant at the 90%  
750 confidence level. Regional averages over Australia are noted at the bottom-left corner of each  
751 panel.